*SF2A 2013*
*L. Cambrésy, F. Martins, E. Nuss and A. Palacios (eds)*

# THE ROLE OF COSMIC RAYS IN THE PROTOSTELLAR DISC FORMATION

M. Padovani[1], P. Hennebelle[2] and D. Galli[3]

**Abstract.** Cosmic rays represent the main actors in regulating the chemical evolution and in setting the ambipolar diffusion time of a molecular cloud. We summarise the processes causing the energy degradation of cosmic rays due to their interaction with molecular hydrogen, also focusing on the magnetic effects that influence their propagation. Making use of magnetic field configurations generated by numerical simulations, we show that the concentration and the wrapping of the field lines in the collapse region lead up to a drop of the cosmic-ray ionisation rate, and consequently of the ionisation fraction, helping to decouple the gas from the magnetic field.

Keywords: ISM: cosmic rays – ISM: clouds, magnetic fields

## 1 Introduction

Cosmic rays (CRs) play a fundamental role in the interaction with the interstellar matter. They affect numerous physical and chemical processes, being responsible for the evolution of molecular clouds and the formation of the first prestellar structures. In fact, when the visual extinction is higher than about 3–4 magnitudes, the UV radiation field becomes too weak to ionise a cloud and CRs become the foremost ionising agents of the densest regions. As a consequence, CRs are accountable for the ignition of the chemistry in the interstellar medium that arises from the atomic and molecular hydrogen ionisation. Being charged particles, CRs are also partially coupled with interstellar magnetic fields so that they act as regulators on the formation of a protostellar disc.

We are witnessing an era of strong development of new telescopes with higher and higher resolution allowing new observing techniques so as to constrain the CR flux at energies lower than about 1 GeV. Observations of $H_3^+$ in diffuse clouds (e.g. Indriolo et al. 2012), detections of $OH^+$ and $H_2O^+$ in low $H_2$ fraction regions (Neufeld et al. 2010, Gerin et al. 2010), enhanced CR ionisation rate ($\zeta^{H_2}$) in molecular clouds close to supernova remnants (Ceccarelli et al. 2011) as well as $\gamma$ luminosity of molecular clouds (e.g. Montmerle 2010) pose the question about how to reconcile the high values of $\zeta^{H_2}$ estimated in diffuse regions with those ones measured in denser clouds that are more than one order of magnitude lower. This problem has been addressed using different strategies, analysing the effects of Alfvén waves on CR streaming (Skilling & Strong 1976, Hartquist et al. 1978, Padoan & Scalo 2005, Rimmer et al. 2012), magnetic mirroring and focusing (Cesarsky & Völk 1978, Chandran 2000, Padovani & Galli 2011, hereafter PG11), or the possible existence of a low-energy flux of CR particles able to ionise diffuse but not dense clouds (Takayanagi 1973, Umebayashi & Nakano 1981, McCall et al. 2003, Padovani et al. 2009, hereafter PGG09).

In the following, we resume our previous studies about the dependence of $\zeta^{H_2}$ on the column density passed through (Sect. 2) and on the magnetic field configuration (Sect. 3). In Sect. 4 we examine the evolution of $\zeta^{H_2}$ for a number of numerical simulations, discussing the variations of $\zeta^{H_2}$ in protostellar discs. In Sect. 5 we summarise our conclusions with an outlook on future prospects.

[1] Laboratoire de Radioastronomie Millimétrique, UMR 8112 du CNRS, École Normale Supérieure et Observatoire de Paris, 24 rue Lhomond, 75231 Paris cedex 05, France
[2] CEA, IRFU, SAp, Centre de Saclay, 91191 Gif-Sur-Yvette, France
[3] INAF–Osservatorio Astrofisico di Arcetri, Largo E. Fermi 5, I–50125 Firenze, Italy

## 2 Column-density effects on the CR ionisation rate

While entering an interstellar cloud, CRs mainly interact with molecular hydrogen and are subject to different energy loss processes depending on their energy and their composition (namely protons, electrons, and heavy nuclei). Table 1 lists the processes degrading the CR spectrum.

The quantity that describes the CR braking for the component $k$, called *energy loss function*, is defined by

$$L_k(E_k) = -\frac{1}{n(\mathrm{H_2})}\left(\frac{\mathrm{d}E_k}{\mathrm{d}\ell}\right) , \tag{2.1}$$

where $n(\mathrm{H_2})$ is the density of the medium in which the particle of energy $E_k$ propagates and $\ell$ is the path length. The spectrum of CR particles of species $k$ at depth $N(\mathrm{H_2})$, $j_k(E_k, N)$, namely the number of particles

Table 1: List of the energy loss processes during the collision between CRs and $\mathrm{H_2}$.

| Energy loss process | CR component affected |
|---|---|
| Coulomb interactions | $p$, $e$ |
| Elastic interactions | $p$ |
| Inelastic interactions | $p$, $e$ |
| Ionisation | $p$, $e$ |
| Bremßtrahlung | $e$ |
| Synchrotron emission | $e$ |
| Inverse Compton scattering | $e$ |
| Pion production | $p$ |
| Spallation | $p$ |

per unit area, time, solid angle, and per energy interval, can be related with the local interstellar spectrum incident on the surface of the cloud, $j_k(E_k, 0)$, using the definition of $L_k(E_k)$. Assuming that (*i*) the direction of propagation of a CR does not change critically inside the cloud (Takayanagi 1973) and that (*ii*) the number of particles is conserved (ignoring electron capture reactions of CR protons with $\mathrm{H_2}$ and He as well as the $\alpha+\alpha$ fusion reactions that form $^6$Li and $^7$Li because of the small cross sections, Meneguzzi et al. 1971), $j_k(E_k, N)$ is related to $j_k(E_k, 0)$ by

$$j_k(E_k, N) = j_k(E_{k,0}, 0)\frac{L_k(E_{k,0})}{L_k(E_k)} \tag{2.2}$$

where $E_{k,0}$ is the initial energy of the CR and $E_k$ is the energy of the CR at depth $N(\mathrm{H_2})$.

In PGG09 we show that even if a local interstellar spectrum is devoid of low-energy particles, a low-energy tail is produced by the slowing-down of CR protons and electrons during their propagation. Our modelling is able to explain the decrease of $\zeta^{\mathrm{H_2}}$ with increasing hydrogen column density computed from observations. In particular, a proton component at low energies, and most likely also an electron component, could be necessary to reproduce the data. Figure 1 is the updated version of Fig. 15 in PGG09 including most recent estimates.

## 3 Magnetic-field effects on the CR ionisation rate

CRs are charged particles and interact with the magnetic field threading a molecular cloud. In PG11 we investigate the propagation of CRs along field lines accounting for magnetic mirroring and focusing that act reducing and amplifying the CR flux, respectively. In fact, assuming the conservation of the kinetic energy of a particle, $E_{\mathrm{kin}} = (\gamma - 1)mv^2$, and of its magnetic momentum, $\mu = \gamma m v^2 \sin^2\alpha/2B$, it is possible to prove that, depending on the initial angle, $\alpha_{\mathrm{ICM}}$, between the particle's velocity and the magnetic field, a CR can cross the entire core or can be bounced out (*mirroring*), leading to a decrease of $\zeta^{\mathrm{H_2}}$. Conversely, supposing the same number of CRs per length of field line and being the CR flux proportional to the density of magnetic field lines per unit area, the CR flux in the cloud must be a factor $\chi = B/B_{\mathrm{ICM}}$ larger than the flux in the intercloud medium (ICM), where $B$ is the magnetic field module (*focusing*). As a consequence, $\zeta^{\mathrm{H_2}}$ will be boosted in regions with higher magnetic field.

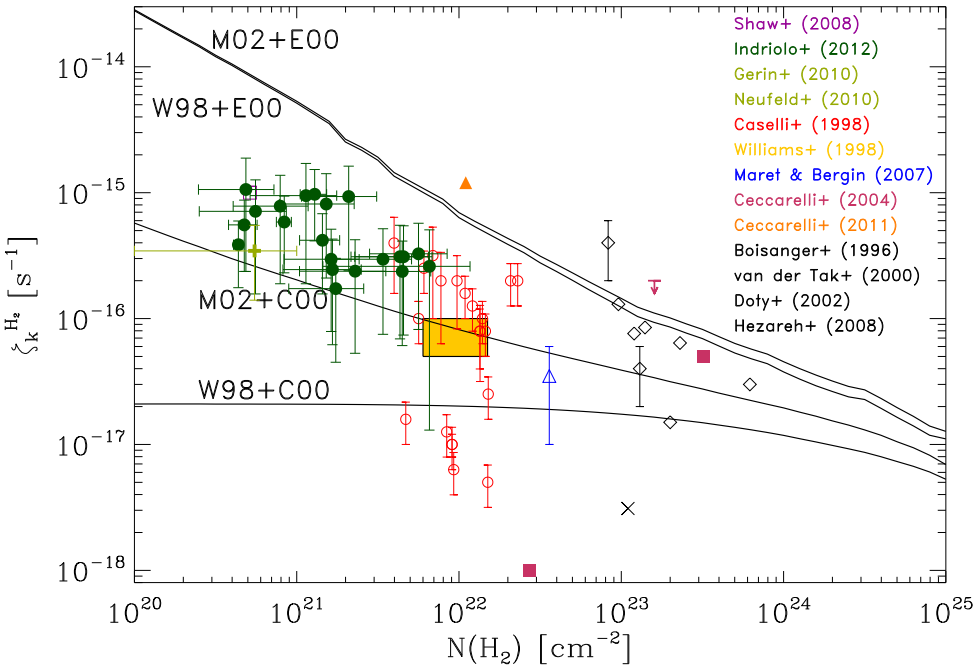


Fig. 1: Total CR ionisation rate, $\zeta^{H_2}$, as function of $N(H_2)$ according to our models (*solid* curves) in comparison with available observational data. Model labels are given in PGG09.

The evolution of the pitch angle along its trajectory is then given by

$$\alpha = \arccos\sqrt{1-\chi+\chi\cos^2\alpha_{\rm ICM}}\,, \tag{3.1}$$

and the column density "seen" by a CR reads

$$N(\alpha) = \int_0^{\ell_{\rm max}(\alpha)} n(\ell)\,{\rm d}\ell\,, \tag{3.2}$$

where $\ell_{\rm max}$ is the maximum depth reached inside the core and $n(\ell)$ is the $H_2$ volume density. If $\alpha$ reaches $\pi/2$, then the particle is bounced back, otherwise, having enough energy, it crosses the core as sketched in Fig. 2.

## 4 CR ionisation in protostellar discs

In Padovani, Hennebelle & Galli (2013b), hereafter PHG13, we check the possibility that a reduction of the CR flux due to the field line twisting in a collapsing cloud can decrease $\zeta^{H_2}$, and then the ionisation fraction. For this purpose, we follow the path of CRs using magnetic field configurations generated by numerical simulations related to a rotating collapsing core (described in PHG13 and detailed in Joos et al. 2012), performed with the AMR code RAMSES (Teyssier 2002, Fromang et al. 2006). We assume the model M02+C00 (see Fig. 1 and PHG13) as "fiducial" spectrum in order to describe $\zeta^{H_2}$ as function of the column density. For each field line and each initial pitch angle $\alpha_{\rm ICM} \in [0, \pi/2)$, we compute $\zeta^{H_2}(\alpha)$ following Padovani, Galli & Glassgold (2013a), hereafter PGG13,

$$\zeta^{H_2}(\alpha) = \frac{\zeta_0^{(\rm low\ N)}\zeta_0^{(\rm high\ N)}}{\zeta_0^{(\rm high\ N)}\left[\dfrac{N(\alpha)}{10^{20}\ {\rm cm}^{-2}}\right]^a + \zeta_0^{(\rm low\ N)}\left[\exp\left(\dfrac{\Sigma(\alpha)}{\Sigma_0}\right)-1\right]}\,, \tag{4.1}$$

where $\Sigma(\alpha) = \mu m_{\rm p} N(\alpha)/\cos\alpha$ is the effective surface density seen by a CR propagating with pitch angle $\alpha$, $m_{\rm p}$ the proton mass, and $\mu = 2.36$ the molecular weight for the assumed fractional abundances of $H_2$ and He.

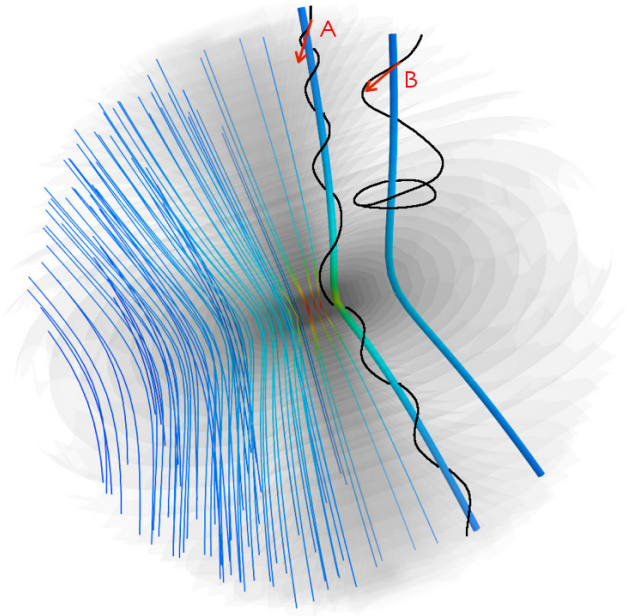


Fig. 2: Sketch of magnetic field lines for a purely poloidal field superposed to density isocontours in grey scale. The two helicoidal *solid black* lines show potential opposite scenarios for the CR path: depending on the CR initial pitch angle, determined by the velocity vector (*red arrows*) and the magnetic field, the particle passes through the core (path A) or goes backwards (path B).

The fitting coefficients of Eq. (4.1) are given in PGG09 and PGG13. In order to evaluate $\zeta^{H_2}$ along a field line, we average the contribution of all the particles with different $\alpha_{\rm ICM}$ over the solid angle. Then we multiply the result by $\chi$ to account for focusing

$$\zeta^{H_2} = \chi \frac{\int \zeta^{H_2}(\alpha)\, \mathrm{d}\Omega_\alpha}{\int \mathrm{d}\Omega_\alpha} = \chi \int_0^{\pi/2} \zeta^{H_2}(\alpha) \sin\alpha \, \mathrm{d}\alpha \,. \tag{4.2}$$

In PHG13 we test a large number of magnetic configurations, varying the initial orientation between the magnetic field direction and the rotation axis, $\alpha_{\rm B,J}$, as well as the mass-to-flux ratio, $\lambda$. Here we focus on two cases leading to the formation of a keplerian disc whose parameters are: ($\mathcal{A}$) $\lambda = 5$ (intermediate magnetisation), $\alpha_{\rm B,J} = \pi/2$ (perpendicular rotator), and $t = 10.756$ kyr; ($\mathcal{B}$) $\lambda = 17$ (weak magnetisation), $\alpha_{\rm B,J} = 0$ (parallel rotator), and $t = 6.620$ kyr, where $t$ is the time after the formation of the first Larson's core*.

Results for the case ($\mathcal{A}$) are presented in the left column of Fig. 3. It is worth noting in the face-on view (upper left panel) a large region of $r \sim 200$ AU and $n \gtrsim 10^9$ cm$^{-3}$ with $\zeta^{H_2} \lesssim 10^{-18}$ s$^{-1}$. Here the ratio between the toroidal component and the magnetic field module, $B_\varphi/B$, is larger than about 0.4. Even lower values, with a minimum of $2 \times 10^{-21}$ s$^{-1}$, are reached in the inner area with an extent of a few tens of AU. This can be also appreciated in the edge-on view (upper right panel) where $\zeta^{H_2}$ is so low that we can assume the gas to be effectively decoupled with the magnetic field. The lower panel shows how the rotation perpendicular to the $y$ axis forces the field lines (initially with a poloidal configuration along the $x$ axis) to wrap around the rotation axis.

A similar set of plots for the case ($\mathcal{B}$) is displayed in the right column of Fig. 3. The high mass-to-flux ratio leads to a weakening of the magnetic field braking, so that the rotation is able to strongly twist the field lines (lower panel). This explains why the decrease of $\zeta^{H_2}$ broadens perpendicularly to the disc plane (upper left panel) and it is not circumscribed to the high-density domain ($n > 10^9$ cm$^{-3}$). In fact, being the field lines very tangled, the magnetic mirror is even more marked, creating a large region along the $x$ axis where $\zeta^{H_2} \sim 10^{-18}$ s$^{-1}$. As for the case ($\mathcal{A}$), the region with $n \gtrsim 10^9$ cm$^{-3}$ and $\zeta^{H_2} \lesssim 10^{-18}$ s$^{-1}$ shows $B_\varphi/B \gtrsim 0.4$.

*It is the core formed in the centre of the pseudo-disc with $n \gtrsim 10^{10}$ cm$^{-3}$ and $r \sim 10 - 20$ AU.

In the $(y, z)$ plane (upper right panel) one can see the presence of the face-on disc and the rapid decrease of $\zeta^{H_2}$ that reaches about $10^{-20}$ s$^{-1}$ in the inner $10^{10}$ cm$^{-3}$ iso-density contour.

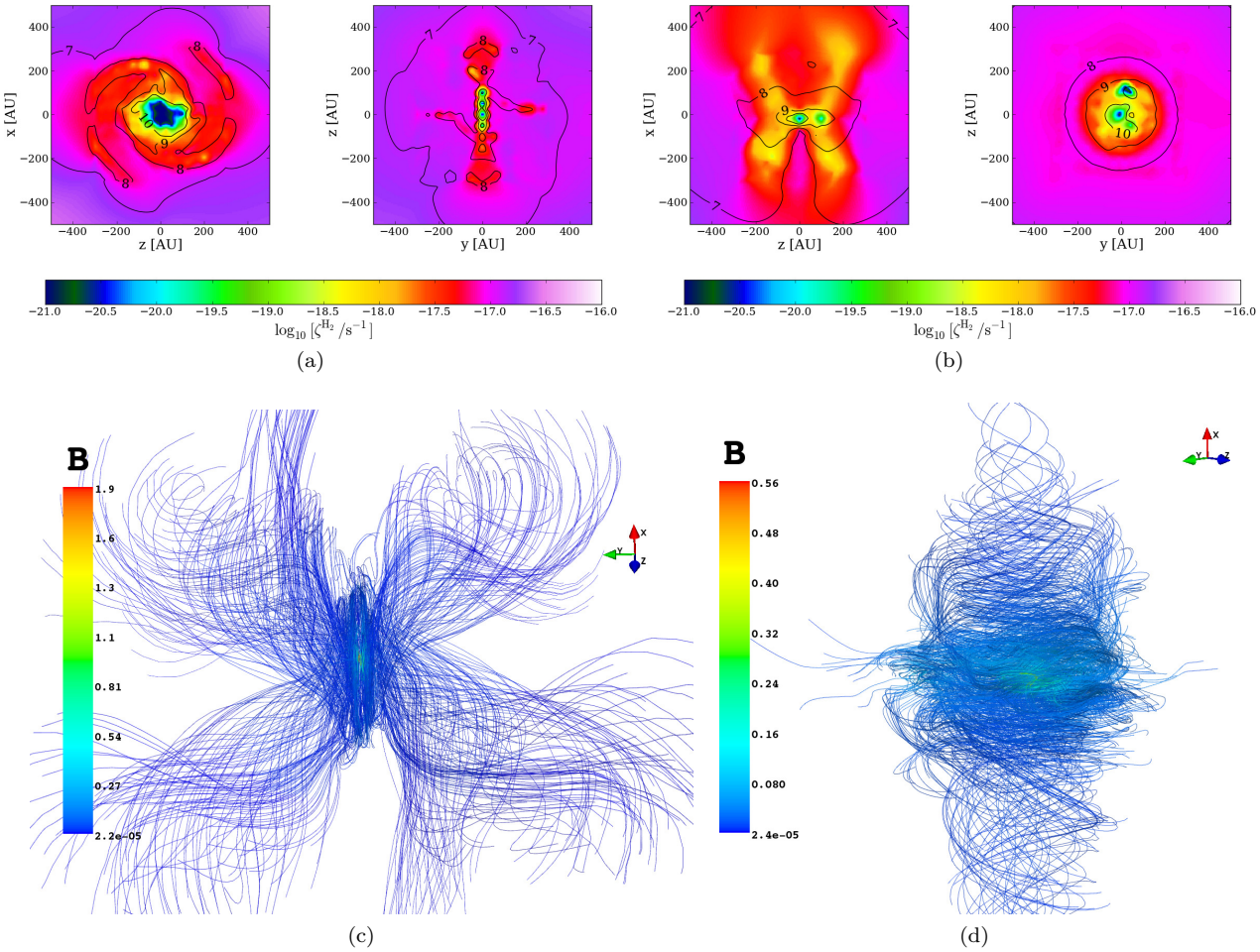


Fig. 3: **Left column:** CR ionisation maps and iso-density contours (*black solid lines*) for the case ($\mathcal{A}$). Upper panels show a slice of a plane parallel to the magnetic field direction (on the left) and of a perpendicular plane (on the right). Both planes contain the density peak and labels show $\log_{10}$ $[n/\mathrm{cm}^{-3}]$. The lower panel shows the magnetic field line morphology in the central 600 AU of the RAMSES data cube. **Right column:** Same as left column plots, but for the case ($\mathcal{B}$).

## 5 Conclusions and future prospects

Magnetic mirroring and focusing set the extent to which CRs can determine the coupling between magnetic fields and the gas. In Sect. 4 we show the importance of accounting for the true path of CRs along magnetic field lines with the inclusion of magnetic effects (see also Sect. 5 in PHG13 for a comprehensive discussion). Being aware of the fact that the correct manner of dealing with CR propagation should be computing their distribution simultaneously with the MHD simulation, we believe that our conclusions represent an important proof of concept. In particular, in the central 100 AU region, the number density is higher than $10^{10}$ cm$^{-3}$ and a $H_2$ column density larger than $10^{25}$ cm$^{-2}$ is promptly reached. This actually means entering the exponential attenuation regime where the CR ionisation rate is independent of the CR spectrum assumed and drops below $10^{-18}$ s$^{-1}$. However, we prove that even in the high-density region, the presence of a magnetic field can reduce $\zeta^{H_2}$ up to a factor larger than 10, well below the ordinarily used value of $10^{-17}$ s$^{-1}$. We conclude that the morphology of the $\zeta^{H_2}$ maps depends both on the density profile and on the magnetic field line configuration.

Non-ideal MHD models predict that magnetic braking becomes inefficient at densities $n > 10^{12}$ cm$^{-3}$, when

magnetic field diffusion becomes faster than the dynamical evolution (Dapp et al. 2012). In our models we observe that the drop in $\zeta^{\mathrm{H_2}}$ takes place in some cases even at lower densities ($n > 10^9$ cm$^{-3}$), resulting in very low ionisation fractions. It will be important to study the consequences of the reduced CR ionisation rate on the magnetic diffusion coefficients (ambipolar, Hall, and Ohm). In order to test this hypothesis, a self-consistent MHD collapse calculation including CR propagation is needed.

## References

Caselli, P., Walmsley, C. M., Terzieva, R., et al. 1998, ApJ, 499, 234

Ceccarelli, C., Dominik, C., Lefloch, B., et al. 2004, ApJ, 607, L51

Ceccarelli, C., Hily-Blant, P., Montmerle, T., et al. 2011, ApJ, 740, L4

Cesarsky, C. J. & Völk, H. J. 1978, A&A, 70, 367

Chandran, B. D. G. 2000, ApJ, 529, 513

Dapp, W. B., Basu, S. & Kunz, M. W. 2012, A&A, 541, A35

de Boisanger, C., Helmich, F. P. & van Dishoeck, E. F. 1996, ApJ, 463, 181

Doty, S. D., van Dishoeck, E. F., van der Tak, F. F. S., et al. 2002, A&A, 389, 446

Fromang, S., Hennebelle, P. & Teyssier, R. 2006, A&A, 457, 371

Gerin, M., De Luca, M., Black, J. et al. 2010, A&A, 518, L110

Hartquist, T. W., Doyle, H. T. & Dalgarno, A. 1978, A&A, 68, 65

Hezareh, T., Houde, M., McCoey, C., et al. 2008, ApJ, 684, 1221

Indriolo, N. & McCall, B. J. 2012, ApJ, 745, 91

Joos, M., Hennebelle, P. & Ciardi, A. 2012 A&A, 543, 128

Maret, S. & Bergin, E. A. 2007, ApJ, 664, 956

McCall, B. J., Huneycutt, A. J., Saykally, et al. 2003, Nature, 422, 500

Meneguzzi, M., Adouze, J. & Reeves, H. 1971, A&A, 15, 377

Montmerle, T. 2010, in ASP Conf. Ser. 422, High Energy Phenomena in Massive Stars, ed. J. Martí, P. L. Luque-Escamilla, & J. A. Combi (San Francisco, CA: ASP), 85

Neufeld, D. A., Goicoechea, J. R., Sonnentrucker, P., et al. 2010, A&A, 521, 10

Padoan, P. & Scalo, 2005, ApJ, 624, L97

Padovani, M., Galli, D. & Glassgold, A. E. 2009, A&A, 501, 619 (PGG09)

Padovani, M. & Galli, D. 2011, A&A, 530, A109 (PG11)

Padovani, M., Galli, D. & Glassgold, A. E. 2013, A&A, 549, C3 (PGG13)

Padovani, M., Hennebelle, P. & Galli, D. 2013, A&A, *in press* (`http://arxiv.org/abs/1310.2158`)

Rimmer, P. B., Herbst, E., Morata, O. et al. 2012, A&A, 537, 7

Skilling, J. & Strong, A. W. 1976, A&A, 53, 253

Takayanagi, M. 1973, PASJ, 25, 327

Teyssier, R. 2002, A&A, 385, 337

Umebayashi, T. & Nakano, T. 1981, PASJ, 33, 617

van der Tak, F. F. S. & van Dishoeck, E. F. 2000, A&A, 358, L79

van der Tak, F. F. S. & van Dishoeck, E. F. & Evans, N. J., II et al. 2000, ApJ, 537, 283

Williams, J. P., Bergin, E. A., Caselli, P. et al. 1998, ApJ, 503, 689